Two-Level DCIM Spatial Green's Functions: Application to Plasmonic Layered Media

Sarah Halawa[1], Alaa K. Abdelmageed[2], and Ezzeldin A. Soliman[1]

[1]Physics Department, School of Sciences and Engineering, The American University in Cairo, AUC Avenue, P. O. Box 74, New Cairo 11835, Egypt
[2]Department of Engineering Mathematics and Physics, Faculty of Engineering, Cairo University, Giza 12211, Egypt

Corresponding author: Ezzeldin A. Soliman (e-mail: esoliman@aucegypt.edu).

ABSTRACT Green's functions of planar layered media are formulated in this paper in the spatial domain. Discrete Complex Image Method (DCIM) is used to transform the spectral Green's functions from the spectral domain back to the spatial domain. Two-level sampling algorithm is adopted which eliminates the need for the analytical treatment of the asymptotes of the spectral Green's functions at high spectral values. The formulation is written to be consistent with the quadruple-dyadic spectral Green's functions recently presented by the authors. These four dyads describe all possible kinds of reactions between currents and fields. The infinitesimal dipole current source can be electric or magnetic oriented either tangential or perpendicular to the layers. All electric and magnetic field components due to these general current sources are obtained. The 34 non-zero elements in these dyads are expressed in terms of 18 spectral Green's functions and 6 spectral coefficients. The presented formulation in this paper allows obtaining the corresponding 18 spatial Green's functions in a straightforward way. This analysis integrated with the preceding spectral analysis leads to quadruple-dyadic spatial Green's functions which may appear in the kernel of any integral equations formulation whatsoever. The implemented two-level DCIM is validated by comparison with published results. Very good agreement is obtained. Then, it has been used to calculate the spatial Green's functions of the basic plasmonic layer structures, which are Insulator/Metal (IM), Insulator/Metal/Insulator (IMI), and Metal/Insulator/Metal (MIM).

INDEX TERMS Green's functions, integral equations, layered media, discrete complex images method, plasmonics.

I. INTRODUCTION

The ability to formulate electromagnetic fields in multilayer media is becoming more and more crucial, as it is required in the analysis and the numerical simulation of microwave, millimeter-wave, and optical integrated circuits, microstrip antennas [1], nano-antennas [2], and transmission line interconnects [3, 4]. Other important situations where such analysis is also vitally needed are electromagnetic scattering [5] and geophysical prospecting. In problems such as the aforementioned scattering, antenna, and transmission line problems, where the currents are not known a priori, the dyadic Green's functions are used to formulate integral equations for the unknown true or equivalent currents. Integral equations are equations where the unknown current quantity appears in the integrand [6].

The integral equations are usually solved using the Method of Moments, MoM. This method is a widely used numerical technique in computational electromagnetics. It can solve the integral equation formulated either in the spectral [7, 8], or the spatial domain [1-4, 9, 10]. In essence, the MoM is a method that transforms any integral equation into a linear system of equations which can be solved via various techniques. The matrix elements resulting from the application of the MoM are multi-fold integrals in general. The spatial domain approach is preferred over the spectral domain approach due to two main reasons: First, working in the spatial domain obviously provides more physical insight to the problem, as one deals with the physical spatial variables x and y instead of the spectral counterparts k_x and k_y. Additionally, the integrands of the MoM matrix elements need to be evaluated over a finite range in the spatial, as opposed to over an infinite range in the spectral domain. However, the only disadvantage of the spatial MoM is the need for transforming the spectral domain Green's functions into the space domain. Unfortunately, this transformation is of Sommerfeld type [11], which is difficult to be performed numerically due to the misbehavior of its integrand, namely the spectral Green's function. Such function suffers from singular behavior, poles and branch points, in addition of being slowly decaying with an asymptotic behavior.

The most direct method for evaluating the Sommerfeld integration is the real-axis numerical integration. Unfortunately, this method is very time consuming, especially because when dealing with multilayer media, these

integrals have to be evaluated repeatedly. Therefore, many methods have been devised to evaluate the Sommerfeld integrals in an efficient and robust manner. The most efficient way to achieve this is to approximate the spectral domain Green's functions in terms of complex exponential images and transforming them back into the spatial domain analytically using a Sommerfeld identity.

In [12] a single closed-form expression for a horizontal electric dipole over a thick substrate backed by a ground plane was derived. The method started by extracting the quasi-static images, the asymptotes, and the Surface Wave Poles (SWPs) of the spectral domain Green's functions and then approximating the remainder by using Prony's method. Consequently, the spatial domain Green's functions were cast into closed forms with analytical representations of the quasi-static terms, SWP contributions and the discrete complex images. Unfortunately, this method still suffered from noise sensitivity and the large number of samples required by Prony's method. Additionally, the geometry specific extraction of the quasi-static terms rendered such technique not perfectly suitable for the development of Computer Aided Design (CAD) tools.

Despite the disadvantages, the technique in [12] was extended to microstrip structures with substrate and superstrate of arbitrary thicknesses [13]. Instead of the original Prony's method, the more efficient least-square Prony's method was used, which helped in tracking fast changes of the spectral domain Green's functions with a reasonable number of exponentials, thus requiring fewer samples. However, the least-square Prony's method still suffered from noise sensitivity and hence required a significant number of trial and error iterations.

To circumvent this problem, another less noise sensitive method for the exponential approximation, the Generalized Pencil Of Function (GPOF) method, was employed in [14] for multilayer geometries with arbitrary thicknesses and sources. In [14] a single-level sampling algorithm in conjunction with the GPOF, the Discrete Complex Image Method (DCIM), was used to cast the spatial domain Green's functions into closed forms. Even though the single-level DCIM was considered to be a marked improvement when compared to all previous attempts, it still suffered from a vital issue: the spectral domain Green's functions needed to be examined in advance in order to decide on the approximation parameters, in particular the number of samples that are needed for this approximation as well as the sampling range. Additionally, to account for fast changes in the spectral domain Green's functions, one had to increase the number of samples which was challenging especially if a large sampling range was needed.

To alleviate such problems that render the former algorithm not generic and consequently not adequate for commercial CAD tools, a two-level sampling algorithm in conjunction with the GPOF, the two-level DCIM, was devised [15]. This algorithm is adopted in this paper. A more fancy extension of the two-level DCIM, is the three-level DCIM devised in [16]. An extra sampling path is added to ensure capturing the contribution of the branch points singularity. In general any additional path may be incorporated in the two-level DCIM technique as long as it adds in capturing the contribution of the singularities of the spectral domain Green's functions. However, the enhancement gained by using three-level is almost unpronounced, if devices with small electrical size are considered. In [17] a spatial domain error metric is incorporated in the two-level DCIM algorithm. This error metric is additionally translated in order to have an analogous error metric in the spectral domain. Additionally, an automatic order selection that is based on the Minimum Description Length (MDL) concept is added to the two-level DCIM algorithm in order to automatically determine the number of exponentials required for approximation to give minimal error. Finally, leakage problems that might occur in the two-level DCIM are dealt with and eliminated. In [25], the accuracy of the DCIM is improved via optimized computation of the poles and residues.

Recently, quadruple-dyadic spectral Green's functions of infinitesimal dipole current sources in planar layered media is presented [18]. The four dyads in [18] carry all kinds of field/current reactions. All components of electric and magnetic fields due to electric/magnetic dipole source with general orientation are obtained through 18 basic spectral Green's functions in terms of 6 spectral coefficients. The formulation presented in this paper is building on the work presented in [18].

The paper is structured as follows. In Section II, two-level DCIM is used in order to transform the quadruple-dyadic spectral Green's functions to the spatial domain. This two-level DCIM is formulated to be consistent with the spectral formulation presented in [18]. Then, numerical examples are presented in Section III to highlight the robustness and accuracy of the implemented procedure. The concentration in the numerical examples is given to plasmonic layered medium owing to the recent interest in this area. Finally, important conclusions of the paper are summed up in Section IV.

II. TWO-LEVEL DCIM FORMULATION

The layer structure under consideration consists of N layers, where each layer is characterized by its permittivity, ε, and permeability, μ. A source is inserted at the interface between jth and $(j+1)$th layer, as shown in Fig. 1. This source can be either Horizontal Electric Dipole (HED), Vertical Electric Dipole (VED), Horizontal Magnetic Dipole (HMD), or Vertical Magnetic Dipole (VMD). It has been demonstrated in [18] that all spectral domain Green's functions in this quadruple-dyadic formulation are are expressed as a summation of a few terms taking the following form:

$$\tilde{G}_{ij}\left(k_\rho, z\right) = \tilde{G}_{ij}\left(k_\rho\right)\, e^{\pm jk_{zi}z} \tag{1}$$

where i and j are the observation and source layer, respectively. To obtain the spatial domain Green's function from its spectral domain counterpart, the following Sommerfeld integral has to be evaluated:

$$G_{ij}\left(\rho, z\right) = \frac{1}{4\pi}\int_{-\infty}^{\infty} dk_\rho k_\rho H_0^{(2)}\left(k_\rho\rho\right)\, \tilde{G}_{ij}\left(k_\rho, z\right)$$

$$= \frac{1}{2\pi}\int_{0}^{\infty} dk_\rho k_\rho J_0\left(k_\rho\rho\right)\, \tilde{G}_{ij}\left(k_\rho, z\right) \tag{2}$$

where G_{ij} and $\tilde{G}_{ij}$ are the spatial and spectral domain Green's functions, respectively. $H_0^{(2)}(.)$ and $J_0(.)$ are the zeroth order Hankel function of the second kind and the zeroth order Bessel function, respectively.

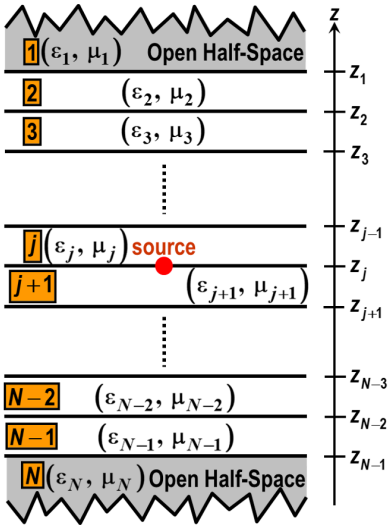

FIGURE 1. Planar multilayered medium carrying an infinitesimal dipole source of the type HED, VED, HMD, or VMD, located at the jth interface.

The integrand of (2) is highly oscillatory and slowly decaying in nature, which renders the computation of this integral computationally very expensive. Furthermore, the spectral domain Green's functions exhibit singular behaviors that make the integration over the real axis a difficult and inefficient task. The singular behavior is mainly due to two main reasons. The first reason is the excitation of surface wave modes in the multilayer structure which manifest themselves as poles located very close to the real axis range $k_\rho : k_0 \to k_m$, where k_m is the maximum of the real parts of the wave numbers of the multilayer structure. As depicted in Fig. 2, SWPs can be found off the real axis if losses are present in the layered medium under consideration. These poles always appear in negative pairs within the complex k_ρ plane [16]. In addition to the physical singularities, i.e. poles, associated with resonance with surface wave modes, spectral Green's functions suffer from another type of singularity, namely branch cuts. These branch cuts are mathematical singularities whose locations are specified according to the parameters of the non-metallic terminal layers [18]. Branch cuts always form traces in the spectral domain that are parallel to the $\Im m\left(k_\rho\right)$ axis, starting from $k_\rho = \pm k_{1,M}$ and extending up to infinity, as shown in Fig. 2, where 1 and M are the upper and lower-most layer, respectively, in the layer structure under investigation.

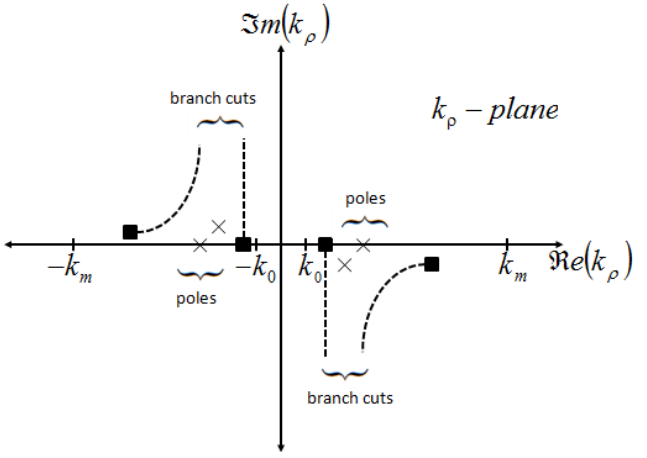

FIGURE 2. Types of singularities of the spectral domain Green's function in the complex k_ρ plane.

To overcome the difficulties of the real-axis numerical integration, a technique referred to as the Discrete Complex Image Method (DCIM) is used. In the DCIM the spectral domain Green's function $\tilde{G}\left(k_\rho\right)$, without the z-dependent exponential function in (1), is approximated by complex exponentials. This enables the analytical evaluation of the Sommerfeld integral (2) by using the following Sommerfeld identity [19]:

$$\frac{e^{-jk_i r}}{r} = -\frac{j}{2}\int_{-\infty}^{\infty} dk_\rho k_\rho H_0^{(2)}\left(k_\rho\rho\right)\frac{e^{-jk_{zi}|z|}}{k_{zi}}$$

$$= -j\int_{0}^{\infty} dk_\rho k_\rho J_0\left(k_\rho\rho\right)\frac{e^{-jk_{zi}|z|}}{k_{zi}} \tag{3}$$

where the spatial distance r is expressed as follows:

$$r = \sqrt{\rho^2 + z^2} \tag{4}$$

The algorithm employed in the two-level DCIM to approximate the spectral domain Green's functions in terms of complex exponentials, is the Generalized Pencil Of Function (GPOF) method [20]. This technique can be looked at as some sort of curve fitting using exponential basis functions, as follows:

$$k_{zi}\tilde{G}\left(k_\rho\right) = \sum_{n=1}^{N} a_n\, e^{\alpha_n t} \tag{5}$$

where N is the number of exponentials sufficient to fit the function with good accuracy, a_n and α_n are the complex residue and exponent, respectively, of the nth expansion term. The number of exponential terms, N, required for accurate curve fitting is determined automatically by the GPOF algorithm by comparing the fitted function with the original up to a certain prespecified number of significant digits. The sampling parameter t is varying linearly from 0 to any maximum value t_m. This sampling parameter can be linked to the independent spectral variable k_ρ using an appropriate sampling law. It can be noticed in (5) that the function expanded using the GPOF is not the Green's function itself, but its product by k_{zi}. This allows one to write the Green's function expansion as a series of exponentials divided by k_{zi}, which facilitates the use of the Sommerfeld identity in (3).

Similar to any other curve fitting method, GPOF samples the function under investigation within the independent variable range of interest. In our case, according to (2), the independent variable is the spectral variable k_ρ, while the range of interest is along the real axis in the interval $(-\infty \to \infty)$ or $(0 \to \infty)$. To avoid the poles, which are located as shown in Fig. 2, a sampling path consisting of two parts is used. This path is shown in Fig. 3. The part of the path at low k_ρ, which is denoted by C_2, is deviated from the real axis in order not to hit the poles. On the other hand, the high k_ρ part of the path, denoted by C_1, is running along the real axis from β_2 till β_1, where no poles are present [15]. These spectral values should be adjusted such that β_2 is larger than k_m, while β_1 should be large enough to capture the asymptotic behavior of the spectral Green's function. It should be noted here that while relatively large number of samples are required along C_2 to capture the rapid variation of the spectral function at low k_ρ, smaller number of samples are needed along C_1 where the function shows a slowly varying asymptotic behavior.

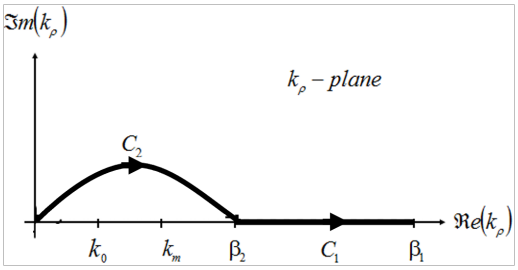

FIGURE 3. Sampling path used in the two-level DCIM in the complex k_ρ plane.

This sampling path is redrawn in the complex k_{zi} plane in Fig. 4, by making use of the following mapping:

$$k_{zi}^2 = k_i^2 - k_\rho^2 \tag{6}$$

Using this mapping, the following relationships between the edges of the sampling paths C_1 and C_2 in the complex k_ρ and k_{zi} planes, can be easily derived:

$$\gamma_1 = \sqrt{\beta_1^2 - k_i^2} \tag{7}$$

$$\gamma_2 = \sqrt{\beta_2^2 - k_i^2} \tag{8}$$

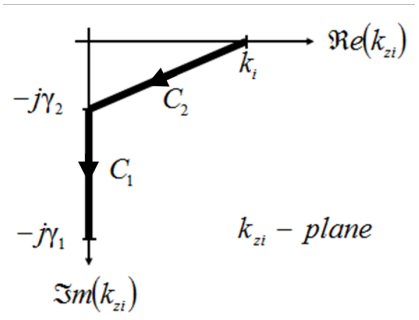

FIGURE 4. Sampling path used in the two-level DCIM in the complex k_{zi} plane.

Comparing the sampling path C_2 in both k_ρ and k_{zi} planes, it is much easier to write the sampling law of C_2 in k_{zi} plane, as it is linear in this plane. GPOF requires the sampling parameter t to vary linearly along the sampling path. The relationship between t and k_{zi} for the two paths C_1 and C_2, can be easily written as follows:

$$k_{zi} = \begin{cases} -j\left[\gamma_2 + (\gamma_1 - \gamma_2)t\right], & (\text{along } C_1) \\ k_i - (k_i + j\gamma_2)t, & (\text{along } C_2) \end{cases}; \quad t: 0 \to 1 \tag{9}$$

This equation can be rewritten, such that the sampling parameter t is expressed in terms of k_{zi}:

$$t = \begin{cases} \dfrac{\gamma_2}{\gamma_2 - \gamma_1} - \dfrac{jk_{zi}}{\gamma_2 - \gamma_1}, & (\text{along } C_1) \\ \dfrac{k_i}{k_i + j\gamma_2} - \dfrac{jk_{zi}}{-\gamma_2 + jk_i}, & (\text{along } C_2) \end{cases} \tag{10}$$

Using GPOF (5) and making use of (10), the spectral domain function $k_{zi}\tilde{G}_1$ along the first level C_1 can be written as follows:

$$k_{zi}\tilde{G}_1(k_\rho) = \sum_{n=1}^{N_1} a_{1n}\, e^{\alpha_{1n} t} = \sum_{n=1}^{N_1} a_{1n}\, e^{\alpha_{1n}\frac{\gamma_2}{\gamma_2 - \gamma_1}}\, e^{-\alpha_{1n}\frac{jk_{zi}}{\gamma_2 - \gamma_1}} \tag{11}$$

Hence,

$$\tilde{G}_1\left(k_\rho\right)=\sum_{n=1}^{N_1} a_{1n}\, e^{\alpha_{1n}\frac{\gamma_2}{\gamma_2-\gamma_1}}\,\frac{e^{-\alpha_{1n}\frac{jk_{zi}}{\gamma_2-\gamma_1}}}{k_{zi}} \tag{12}$$

The spectral function $\tilde{G}_1$ represents the asymptotic behavior of the corresponding Green's function $\tilde{G}$. Hence, $\tilde{G}_1$ matches $\tilde{G}$ at high spectral values. A relatively small number of samples is needed in this level to achieve good curve fitting via GPOF, where the spectral function is slowly varying in this level.

Now, the spectral Green's function has to be investigated along the low spectral values, i.e. along C_2. The extrapolation of $\tilde{G}_1$ along the second level is not expected to match the original function $\tilde{G}$. Hence, another GPOF fitting is needed to represent the difference between $\tilde{G}$ and the extrapolation of $\tilde{G}_1$ along the sampling path C_2. Employing (10) and (5), one can write:

$$k_{zi}\tilde{G}_2\left(k_\rho\right)=k_{zi}\left(\tilde{G}-\tilde{G}_1\right)=\sum_{n=1}^{N_2} a_{2n}\, e^{\alpha_{2n}t}$$

$$=\sum_{n=1}^{N_2} a_{2n}\, e^{\alpha_{2n}\frac{k_i}{k_i+j\gamma_2}}\, e^{-\alpha_{2n}\frac{jk_{zi}}{-\gamma_2+jk_i}} \tag{13}$$

which is equivalent to:

$$\tilde{G}_2\left(k_\rho\right)=\sum_{n=1}^{N_2} a_{2n}\, e^{\alpha_{2n}\frac{k_i}{k_i+j\gamma_2}}\,\frac{e^{-\alpha_{2n}\frac{jk_{zi}}{-\gamma_2+jk_i}}}{k_{zi}} \tag{14}$$

Since the spectral function is showing rapid variation at low spectral values, relatively large number of samples are needed to represent the function with good accuracy along C_2. Since $\tilde{G}_2=\tilde{G}-\tilde{G}_1$, the extrapolation of $\tilde{G}_2$ should vanish along C_1, as $\tilde{G}$ and $\tilde{G}_1$ match each other at high spectral values, assuming accurate curve fitting is performed along the first level.

Finally, a closed-form expression for the spectral domain Green's function along the entire spectral range, i.e. along C_2 and C_1 together, can be obtained by adding (12) and (14):

$$\tilde{G}\left(k_\rho\right)=\tilde{G}_1+\tilde{G}_2=\sum_{n=1}^{N_1} a_{1n}\, e^{\alpha_{1n}\frac{\gamma_2}{\gamma_2-\gamma_1}}\,\frac{e^{-\alpha_{1n}\frac{jk_{zi}}{\gamma_2-\gamma_1}}}{k_{zi}}+$$

$$\sum_{n=1}^{N_2} a_{2n}\, e^{\alpha_{2n}\frac{k_i}{k_i+j\gamma_2}}\,\frac{e^{-\alpha_{2n}\frac{jk_{zi}}{-\gamma_2+jk_i}}}{k_{zi}} \tag{15}$$

Now, the complete spectral domain function including the z-dependent exponential function can be obtained by substituting (15) into (1):

$$\tilde{G}\left(k_\rho,z\right)=\sum_{n=1}^{N_1} a_{1n}\, e^{\alpha_{1n}\frac{\gamma_2}{\gamma_2-\gamma_1}}\,\frac{e^{-jk_{zi}\left(\frac{\alpha_{1n}}{\gamma_2-\gamma_1}\mp z\right)}}{k_{zi}}+$$

$$\sum_{n=1}^{N_2} a_{2n}\, e^{\alpha_{2n}\frac{k_i}{k_i+j\gamma_2}}\,\frac{e^{-jk_{zi}\left(\frac{\alpha_{2n}}{-\gamma_2+jk_i}\mp z\right)}}{k_{zi}} \tag{16}$$

Substituting (16) into (2) and making use of the Sommerfeld identity (3) and the spatial relation (4), the spatial domain Green's function can be fully expressed in closed-form, as follows:

$$G\left(\rho,z\right)=\sum_{n=1}^{N_1} a_{1n}\, e^{\alpha_{1n}\frac{\gamma_2}{\gamma_2-\gamma_1}}\,\frac{e^{-jk_i\sqrt{\rho^2+\left(\frac{\alpha_{1n}}{\gamma_2-\gamma_1}\mp z\right)^2}}}{\sqrt{\rho^2+\left(\frac{\alpha_{1n}}{\gamma_2-\gamma_1}\mp z\right)^2}}$$

$$+\sum_{n=1}^{N_2} a_{2n}\, e^{\alpha_{2n}\frac{k_i}{k_i+j\gamma_2}}\,\frac{e^{-jk_i\sqrt{\rho^2+\left(\frac{\alpha_{2n}}{-\gamma_2+jk_i}\mp z\right)^2}}}{\sqrt{\rho^2+\left(\frac{\alpha_{2n}}{-\gamma_2+jk_i}\mp z\right)^2}} \tag{17}$$

This expression can be looked at as the contribution from N_1 and N_2 sources, images, located at complex distances along the z-axis which is perpendicular to the layer structure. Hence, this method is referred to as the Discrete Complex Image Method (DCIM). All the quadruple-dyadic spectral Green's functions presented in [18] can be treated using the technique illustrated in this section in order to obtain the corresponding quadruple-dyadic spatial Green's functions.

III. NUMERICAL RESULTS

In order to have a good understanding of the numerical results presented in this section, it is important to classify the contribution of the spectral function singularities, such as poles and branch cuts, and the asymptotes of the spectral Green's function, to the spatial function. For large spatial distances, i.e. in the far-field, the frequency of oscillation of the Bessel function in (2) is high. Consequently, only the fast variation in the spectral function will contribute to the far-field. The rapid spectral variation is occurring around the poles and branch points. Hence, the singularities in the spectral function have the major contribution to the far-field [26]. Physically, the surface wave modes, i.e. poles of the spectral function, are capable of travelling relatively large distance through the layer structure, which gives rise to dominant far-field contribution. On the other hand, the slowly decaying asymptotic behavior of the spectral function

has a minor contribution to the far-field. This asymptotic behavior is attributed physically to the multiple reflections at the interfaces of the layer structure. Such contribution is expected to die out as the observation point gets laterally far from the source point. Hence, the asymptotic contribution is mainly confined to the near-field region [26].

Since the sampling path C_2 is deviated away from the real k_ρ axis for the purpose of avoiding singularities, the presented DCIM is very efficient for electrically small devices. If large devices are of interest, such as antenna arrays, special interest should be given to the contribution of the poles and branch cuts. In that case, the singularities should be subtracted from the spectral function and their contribution should be added analytically to the spatial function. This contribution represents the major part of the Green's function when the mutual coupling between elements of an array, located relatively far from each other, is to be calculated [21].

In this section, numerical results for spatial domain Green's functions are obtained from their spectral counterpart via the two-level DCIM illustrated in the previous section. We start by validating the proposed formulation by comparison with results published in literature for a conventional dielectric/metallic layered medium in the microwave range of frequency. The obtained spatial domain Green's functions are also validated indirectly via using them by an in-house integral equations solver to analyze plasmonic nano-antennas in [2, 18]. After that, the concentration will be given to plasmonic layered media, in which metallic layers are present and operating in the optical frequency range where they behave like plasma. Specifically, spatial Green's functions for Insulator/Metal (IM), Insulator/Metal/Insulator (IMI), and Metal/Insulator/Metal (MIM) layer structures are considered. Several applications utilizing plasmonic layer structures can be mentioned, such as plasmonic/optical nano antennas [27, 28], sensors [29], and filters [30].

The nomenclature used for the different Green's functions considered in the following subsections is the same as that adopted in [18]. The superscript of any of the spectral domain Green's functions consists of two parts. The first part specifies the type of the field to be observed and its polarization being either vertical (z) or transversal-to-z (t). The second part describes the type and orientation of the current source that generates this field. If the link between a field and a current in the quadruple-dyadic matrices of [18] requires two different spectral Green's functions, subscripts A and B are used to differentiate between them.

A. Two Dielectric Slabs Backed by PEC

The layered structure studied in [14] with a HMD placed at the top-most interface is investigated in this subsection. The layered structure, as shown in Fig. 5, consists of the first layer being free-space, the second layer being a dielectric of $\varepsilon_r = 2$ and thickness d = 1.5 mm, the third layer being another dielectric of $\varepsilon_r = 10$ and thickness $d = 0.75$ mm, and the bottom-most layer being a Perfect Electric Conductor (PEC). The field point is chosen to be at the aforementioned interface carrying the source, where the tangential magnetic field is required. Two spectral Green's functions are needed here, which are $\tilde{G}_{A,11}^{H_t,M_t}$ and $\tilde{G}_{B,11}^{H_t,M_t}$. The latter function $\tilde{G}_{B,11}^{H_t,M_t}$ calculated at frequency of 1 GHz is plotted in the complex k_ρ plane in Fig. 6. From this figure, the two-level DCIM parameters, β_1 and β_2, are deduced to be $\beta_2 = 5k_0$ and $\beta_1 = 100k_0$, respectively. The corresponding sampling paths C_2 and C_1 are shown in Fig. 6(a) and 6(b), respectively. It is clear that C_2 surpasses the problematic behavior of the spectral function, while C_1 extends far enough for the spectral function to die out in order to capture its asymptotic behavior. The number of samples taken along C_1 and C_2 are 25 and 100, respectively. Based on these sampling paths' parameters, the spatial Green's functions needed to calculate the tangential magnetic field at the field point due to the HMD located at the source point, $G_{A,11}^{H_t,M_t}$ and $G_{B,11}^{H_t,M_t}$, are obtained and plotted in Figs. 7(a) and 7(b), respectively. These calculated functions are compared to those published in [14]. Perfect agreement can be observed.

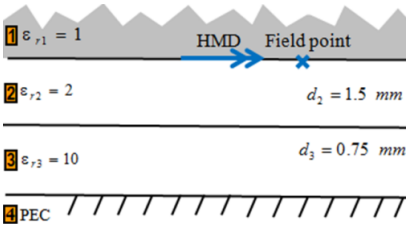

FIGURE 5. Two dielectric slabs backed by PEC showing the source type and location in addition to the field point.

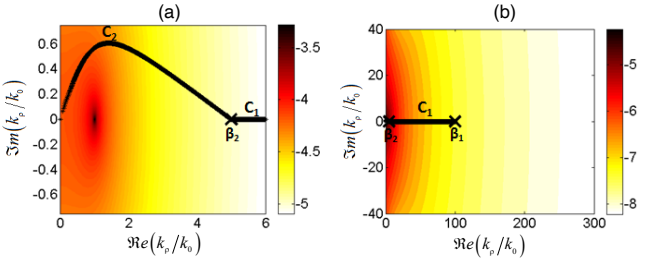

FIGURE 6. $\log_{10}\left|\tilde{G}_{B,11}^{H_t,M_t}\right|$ of the HMD in Fig. 5 along the complex k_ρ plane showing: (a) sampling path C_2 and, (b) sampling path C_1; $\beta_2 = 5k_0$ and $\beta_1 = 100k_0$; f = 1 GHz.

B. Insulator/Metal (IM)

In this subsection, the basic plasmonic structure is considered, namely the Insulator/Metal (IM) structure. An Ag/SiO_2 structure, with silver modeled by the lossless Drude model, is investigated at a free-space wavelength of 619.83 nm, which corresponds to a frequency of 484 THz. This structure has been previously investigated in [22]. The multilayer stack with constitutive parameters is depicted in Fig. 8 and can be summarized as follows: the first layer is

silver with $\varepsilon_r = -7.4716$ and the second is a SiO_2 dielectric with $\varepsilon_r = 2.1250$. A HED source is inserted 100 nm above the metal-dielectric interface to emulate a nano metallic strip on top of a metal half-space. The field point is chosen to be at the source position.

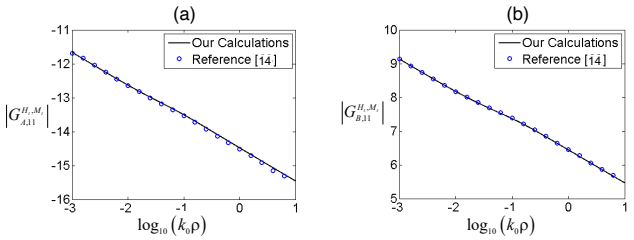

FIGURE 7. Spatial domain Green's functions of the HMD in Fig. 5 versus the spatial distance: (a) $\left|G_{A,11}^{H_t,M_t}\right|$ and (b) $\left|G_{B,11}^{H_t,M_t}\right|$; f = 1 GHz.

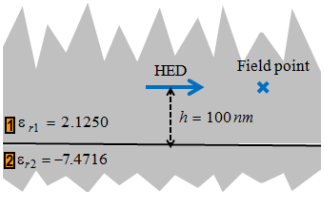

FIGURE 8. Geometry of the IM structure under consideration showing the source type and location in addition to the field point.

The parameters for running the two-level DCIM are deduced from the contour plots of the spectral domain Green's function of this structure, $\tilde{G}_{B,11}^{E_t,J_t}$, which is depicted in Fig. 9(a). A surface wave pole can be easily seen in Fig. 9(a) on the real axis with propagation constant slightly less than $2k_0$. Although the layer structure is formed from two layers with a single interface, it has a natural surface wave mode owing to the negative real permittivity of silver at the selected optical frequency. For the conventional layer structures at the microwave range of frequency, at least three layers and two interfaces are needed for surface wave modes to exist.

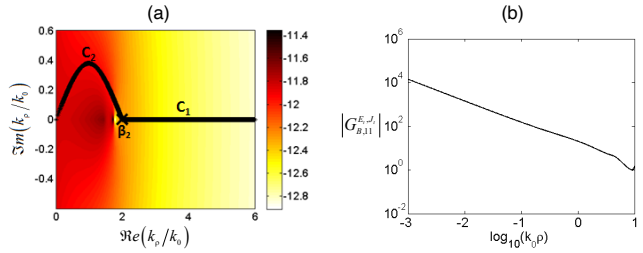

FIGURE 9. (a) $\log_{10}\left|\tilde{G}_{B,11}^{E_t,J_t}\right|$ of the HED in Fig. 8 along the complex k_ρ plane showing sampling paths; $\beta_2 = 2k_0$ and $\beta_1 = 100k_0$; f = 484 THz. (b) Spatial domain counterpart $\left|G_{B,11}^{E_t,J_t}\right|$ versus the spatial distance.

The sampling parameters are $\beta_2 = 2k_0$, $\beta_1 = 100k_0$, and the number of samples taken along C_1 and C_2 are 25 and 100, respectively. The sampling path C_2 is shown completely, while C_1 is shown partially in Fig. 9(a). The corresponding spatial Green's function $G_{B,11}^{E_t,J_t}$ is depicted in Fig. 9(b).

C. Insulator/Metal/Insulator (IMI)

Adding a dielectric layer to the previous IM structure converts it to an Insulator/Metal/Insulator (IMI) structure, which represents another basic plasmonic multilayer stack. In this subsection a metallic silver layer inserted between two insulating free-space layers, which is the structure studied in [23], is examined. The metal is still modeled using the Drude model at an operational frequency of 795.8 THz. The description of the multilayer stack is illustrated in Fig. 10 with the first layer being free-space, the second layer being silver with $\varepsilon_{r2} = -4.499$, and a thickness d_2 = 50 nm, and the third layer being free-space. A HMD source is inserted at the upper-most metal-dielectric interface. The parameters for the two-level DCIM are deduced from the spectral function $\tilde{G}_{B,11}^{H_t,M_t}$ depicted in Fig. 11(a). These parameters are $\beta_2 = 2k_0$, $\beta_1 = 100k_0$, and a number of samples of 25 and 100 along C_1 and C_2, respectively. The spatial function counterpart, $G_{B,11}^{H_t,M_t}$, is plotted in Fig. 11(b) versus the spatial distance.

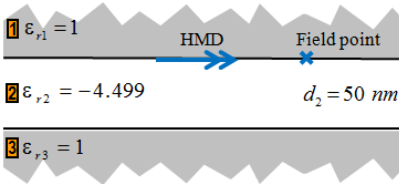

FIGURE 10. Geometry of the IMI structure under consideration showing the source type and location in addition to the field point.

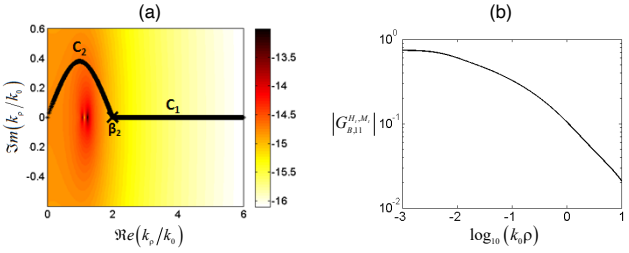

FIGURE 11. (a) $\log_{10}\left|\tilde{G}_{B,11}^{H_t,M_t}\right|$ of the HMD in Fig. 10 along the complex k_ρ plane showing sampling paths; $\beta_2 = 2k_0$ and $\beta_1 = 100k_0$; f = 795.8 THz. (b) Spatial domain counterpart $\left|G_{B,11}^{H_t,M_t}\right|$ versus the spatial distance.

D. Metal/Insulator/Metal (MIM)

On the other hand, adding a metallic layer to the basic IM structure converts it to a Metal/Insulator/Metal (MIM) structure, which represents the third commonly used plasmonic multilayer stack. The MIM layered structure considered in [23] is revisited in this subsection. As shown

in Fig. 12 it consists of a free-space core with a thickness d_2 = 50 nm, which is sandwiched between two silver claddings of $\varepsilon_{r1} = \varepsilon_{r3} = -3.4720 - 0.1864i$ operating at 795.8 THz. This directly implies that the metal is not modeled by the lossless Drude formula anymore, but by the empirical optical constants [24]. A HED source is inserted at the middle of the core, and it is required to calculate the tangential electric field at the same position. The spectral function $\tilde{G}_{B,22}^{E_t,J_t}$ associated with this current/field interaction is plotted in the $\Re e\left(k_\rho\right)$ - $\Im m\left(k_\rho\right)$ plane in Fig. 13(a). Adjusting the DCIM parameters to $\beta_2 = 2.5k_0$, $\beta_1 = 100k_0$ results in the sampling paths C_1 and C_2 shown partially and fully, respectively, in this figure. As before, 25 and 100 samples along C_1 and C_2 , respectively, are sufficient for good curve fitting. The spatial domain Green's function $G_{B,22}^{E_t,J_t}$ calculated using the two-level DCIM is plotted in Fig. 13(b) versus the spatial distance.

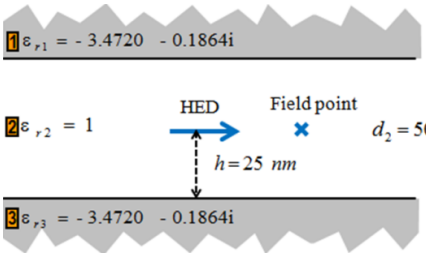

FIGURE 12. Geometry of the MIM structure under consideration showing the source type and location in addition to the field point.

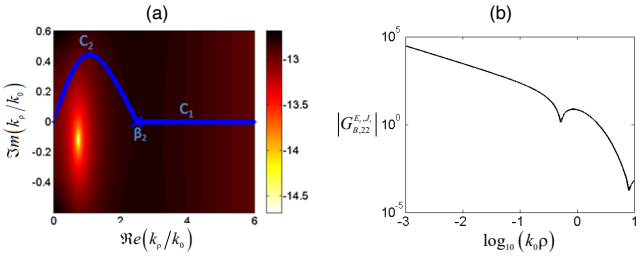

FIGURE 13. (a) $\log_{10}\left|\tilde{G}_{B,22}^{E_t,J_t}\right|$ of the HED in Fig. 12 along the complex k_ρ plane showing sampling paths; $\beta_2 = 2.5k_0$ and $\beta_1 = 100k_0$; f = 795.8 THz. (b) Spatial domain counterpart $\left|G_{B,22}^{E_t,J_t}\right|$ versus the spatial distance.

IV. CONCLUSION

Inverse Fourier transformation of the Green's functions from the spectral to the spatial domain is performed in this paper. The formulation is written in a way to complement the corresponding quadrupole-dyadic spectral formulation. With this integration, it is possible to formulate integral equations for any electromagnetic problem that could exist. The adopted technique which is based on the two-level DCIM is applied successfully on a number of plasmonic layer structures of practical importance.

REFERENCES

[1] E. A. Soliman, M. H. Bakr, and N. K. Nikolova, "Neural Networks – Method of Moments (NN-MoM) for the efficient filling of the coupling matrix," *IEEE Transactions on Antennas and Propagation*, vol. 52, pp. 1521-1529, June 2004.

[2] E. M. Mahdy, A. K. Abdelmageed, and E. A. Soliman, "Integral equation formulation for planar plasmonic structures with finite thickness in layered media," *IEEE Photonics Journal*, vol. 14, pp. 1-9, April 2022.

[3] M. O. Sallam, G. A. E. Vandenbosch, G. Gielen, and E. A. Soliman, "Generalized mode solver for plasmonic transmission lines embedded in layered media based on the method of moments," *Computer Physics Communications*, vol. 233, June 2018.

[4] E. A. Soliman, G. A. E. Vandenbosch, E. Beyne, and R. P. Mertens, "Full-wave analysis of multiconductor multislot planar guiding structures in layered media," *IEEE Transactions on Microwave Theory and Techniques*, vol. 51, pp. 874-886, March 2003.

[5] A. A. Sakr, E. A. Soliman, and A. K. Abdelmageed, "A Surface Integral Equation Formulation for Electromagnetic Scattering from a Conducting Cylinder Coated with Multilayers of Homogeneous Materials," *Journal of Applied Physics*, vol. 116, 054902, 2014.

[6] J. L. Volakis and K. Sertel, *Integral Equation Methods for Electromagnetics. Raleigh*, NC, USA: SciTech Publishing, 2012.

[7] G. Cano, F. Medina, and M. Horno, "Efficient spectral domain analysis of generalized microstrip lines in stratified media including thin, anisotropic, and lossy substrates," *IEEE Transactions on Microwave Theory and Techniques*, vol. 40, pp. 217-227, Feb. 1992.

[8] T. Uwano and T. Itoh, "Spectral domain approach," in *Numerical Techniques for Microwave and Millimeter-Wave Passive Structures*, New York: John Wiley & Sons, 1989, pp. 335-379.

[9] N. Fache and D. De Zutter, "Rigorous full-wave space-domain solution for dispersive microstrip lines," *IEEE Transactions on Microwave Theory and Techniques*, vol. 36, pp. 731-737, Apr. 1998.

[10] C-I G. Hsu, R. F. Harrington, K. A. Michaliski, and D. Zheng, "Analysis of multiconductor transmission lines of arbitrary cross section in multilayered uniaxial media," *IEEE Transactions on Microwave Theory and Techniques*, vol. 41, pp. 70-78, Jan. 1993.

[11] A. Sommerfeld, *Partial Differential Equations in Physics*, New York: Academic, 1949.

[12] Y. L. Chow, J. J. Yang, D. G. Fang, and G. E. Howard, "A closed-form spatial Green's function for the thick microstrip substrate," *IEEE Transactions on Microwave Theory and Techniques*, vol. 39, pp. 588-592, Mar. 1991.

[13] I. Park, R. Mittra and M. I. Aksun, "Numerically efficient analysis of planar microstrip configurations using closed-form Green's functions," *IEEE Transactions on Microwave Theory and Techniques*, vol.43, pp. 394-400, Feb. 1995.

[14] G. Dural and M. I. Aksun, "Closed-form Green's functions for general sources and stratified media," *IEEE Transactions on Microwave Theory and Techniques*, vol. 43, pp. 1545-1552, July 1995.

[15] M. I. Aksun, "A robust approach for the derivation of closed-form Green's functions," *IEEE Transactions on Microwave Theory and Techniques*, vol. 44, pp. 651-658, May 1996.

[16] A. Alparslan, M. I. Aksun and K. A. Michalski, "Closed-form Green's functions in planar layered media for all ranges and

materials," *IEEE Transactions on Microwave Theory and Techniques*, vol. 58, pp. 602-613, Mar. 2010.

[17] E. P. Karabulut, A. T. Erdogan and M. I. Aksun, "Discrete complex image method with spatial error criterion and automatic order selection," in *IEEE International Symposium on Antennas and Propagation*, Spokane, Washington, pp. 1577-1580, 2011.

[18] S. Halawa, E. M. Mahdy, A. K. Abdelmageed, and E. A. Soliman, "Quadruple-Dyadic Spectral Green's Functions of Current Sources in Planar Layered Media: Application to Plasmonic Layer-Structures," *IEEE Photonics Journal*, vol. 14, pp. 1-12, June 2022.

[19] W. C. Chew, *Waves and Fields in Inhomogeneous Media*. New York, NY, USA: Wiley, 1995.

[20] Y. Hua and T. K. Sarkar, "Generalized pencil-of-function method for extracting poles of an EM system from its transient response," *IEEE Transactions on Antennas and Propagation*, vol. 37, pp. 229-234, Feb. 1989.

[21] G. A. E. Vandenbosch and F. J. Demuynck, "The expansion wave concept- Part II: A new way to model mutual coupling in microstrip arrays," *IEEE Transactions on Antennas and Propagation*, vol. 46, pp. 407-413, March 1998.

[22] J. A. Dionne, L. A. Sweatlock, H. A. Atwater and A. Polman, "Planar metal plasmon waveguides: frequency-dependent dispersion, propagation, localization, and loss beyond the free electron model," *Physical Review B*, vol. 72, Aug. 2005.

[23] S. A. Maier, *Plasmonics: Fundamentals and Applications*. New York: Springer Science, 2007.

[24] P. B. Johnson and R. W. Christy, "Optical constants of the noble metals," *Physical Review B*, vol. 6, pp. 4370-4379, July 1972.

[25] S. D. Gedney, N. Hendijani, J. C. Young, and R. J. Adams, "Electrostatic boundary integral method for 3D structures in a layered conducting medium," *IEEE Journal on Multiscale and Multiphysics Computational Techniques*, vol. 9, pp. 218-227, June 2024.

[26] F. J. Demuynck, G. A. E. Vandenbosch, and A. R. Van de Capelle, "The expansion wave concept-Part I: Efficient calculation of the spatial Green's functions in a stratified dielectric medium," *IEEE Transactions on Antennas and Propagation*, vol. 46, pp. 397-406, March 1998.

[27] A. Singh, S. Kavitha, V. D. Shastrimath, and M. Aneesh, "A review on design, development and characterization of plasmonic nano-antenna for photonic applications" *Journal of Optical Communications*, vol. 45, pp. s2387-s2400, 2024.

[28] Dong, T., He, J., Xu, Y., *Design of Optical Antennas and Arrays. In: Photonic Integrated Phased Array Technology*, 2024, Springer.

[29] M. M. Gad, Y. M. El Batawy, and M. O. Sallam, "Particle swarm optimization of high Q factor interdigitated E-shaped metamaterial for refractive index sensing," *Optical and Quantum Electronics*, vol. 56, p. 1799, Oct. 2024.

[30] N. Karani, A. Abbasi, and M. Danaie, "Band-pass and band-stop plasmonic filters based on Wilkinson power divider structure," *Plasmonics*, vol. 19, pp. 733-742, Sept. 2023.